**Supplementary Material for "Timing of Martian Core Formation from Models of Hf–W Evolution Coupled with *N*-body Simulations"**

M. C. Brennan, R. A. Fischer, F. Nimmo, D. P. O'Brien

**Contents of this File**

Text S1

Figures S1–S4

Tables S1–S4

Supplementary References

**Text S1**

The Martian mantle (i.e., Shergottite source) $f^{\mathrm{Hf/W}}$ used in this study (2.0 ± 0.4, Table S4) is different than the value (~3.4) reported by Foley et al. (2005) and Dauphas & Pourmand (2011) and used in some models of Martian Hf–W evolution (e.g., Morishima et al., 2013). We use the $f^{\mathrm{Hf/W}}$ of Kleine & Walker (2017), which agrees with the value reported by Jacobsen (2005) and is the most recent published estimate. The difference between these values is not due to discrepancies in Martian meteorite measurements; in fact, the Kleine & Walker (2017) value derives from the bulk $(\mathrm{Hf/W})_{Mars}$ of Dauphas & Pourmand (2011). Rather, the difference arises from the $\left(^{180}\mathrm{Hf}/^{184}\mathrm{W}\right)_{CHUR}$ value used (Equation 2). Dauphas & Pourmand (2011) use a CHUR composition defined as a Mars-like mixture of meteoritic sources (Lodders & Fegley, 1997), rather than a CI-like value as in Kleine & Walker (2017) or Nimmo & Kleine (2007). Since the distinction is in a constant reference ratio, the actual implied timescale of accretion is identical for either value of $f^{\mathrm{Hf/W}}$. A body that differentiated at some time after CAI will reach a fixed final $\varepsilon_{182\mathrm{W}}$ regardless of which $f^{\mathrm{Hf/W}}$ is used because the implied initial $\left(^{182}\mathrm{W}/^{180}\mathrm{Hf}\right)_{mantle}$ is the same in each case.

**Figure S1**

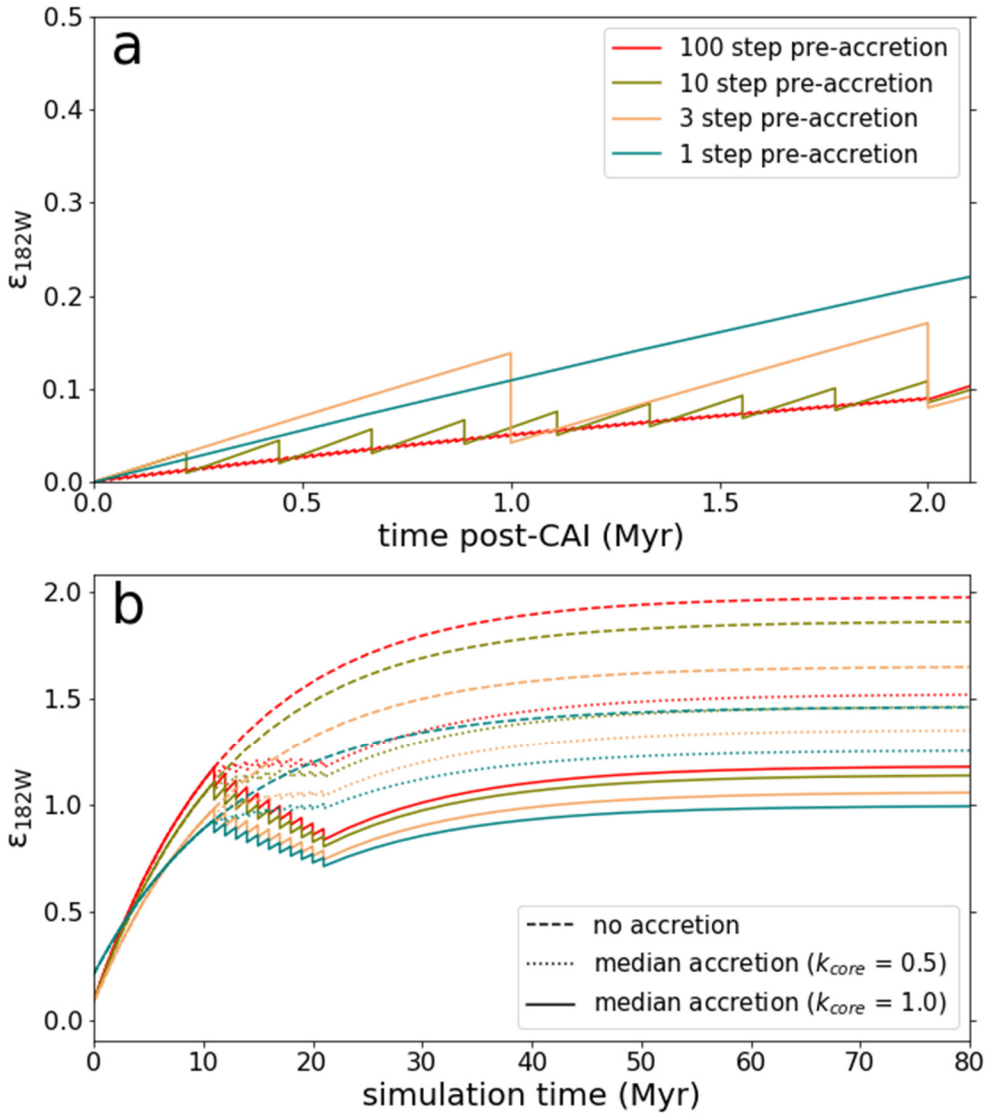


Effect of "pre-accretion" (i.e., oligarchic growth before the *N*-body simulation begins) shown by the evolution of a single embryo with variable prescribed pre-accretion history. Pre-accretion (**a**) consists of homogenous growth steps ($k_{core}$ = 1.0) evenly distributed over the 2 Myr period between CAI condensation and the start of the *N*-body simulation. The effect of increasing the number of steps becomes negligible beyond 100 steps. At later times (**b**), the embryo experiences either no accretion (dashed curves) or a synthetic accretion history based on the median of the Mars analogs (11 planetesimal impactors, 95% mass reached 18 Myr after simulation start; Table S2) with $k_{core}$ = 0.5 (dotted curves) or $k_{core}$ = 1.0 (solid curves). The maximum possible effect of pre-accretion is ~0.5 ε units, and the effect is substantially smaller for most analogs.

**Figure S2**

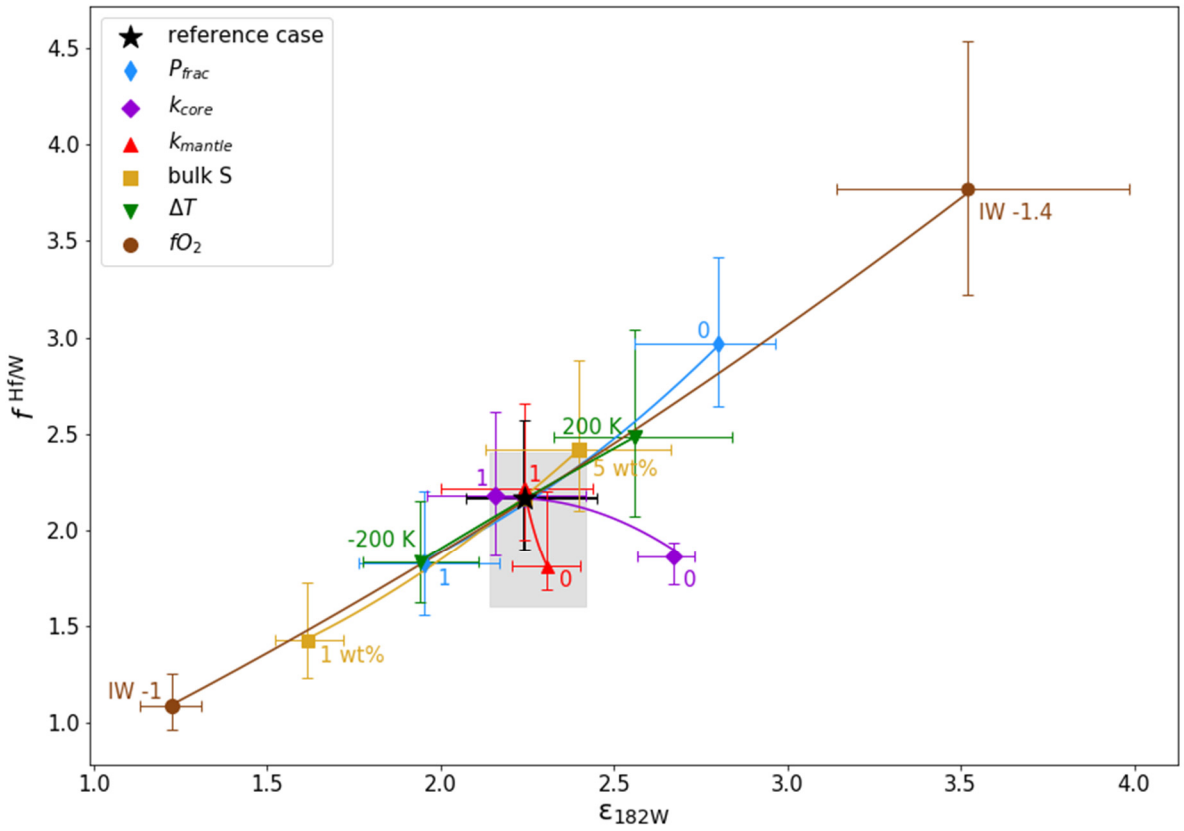


Alternate version of Figure 4 using the W metal–silicate partitioning parameterization of Siebert et al. (2011) (Table S2). Here, the "reference case" parameters are $P_{frac}$ = 0.6, $k_{core}$ = 0.85, $k_{mantle}$ = 0.4, S = 3.5 wt%, $\Delta T$ = 0, and $fO_2$ = IW–1.22. Contrasted with the Jennings et al. (2021) parameterization, this version has generally more siderophile W, a decreased sensitivity to $\Delta T$, an inverted effect of $P_{frac}$, and a larger $k_{core}$ effect on $\varepsilon_{182W}$. The shaded grey region indicates the uncertainty range of measured Martian Shergotty-source values. Symbols denote the median of all analogs and error bars indicate interquartile ranges.

**Figure S3**

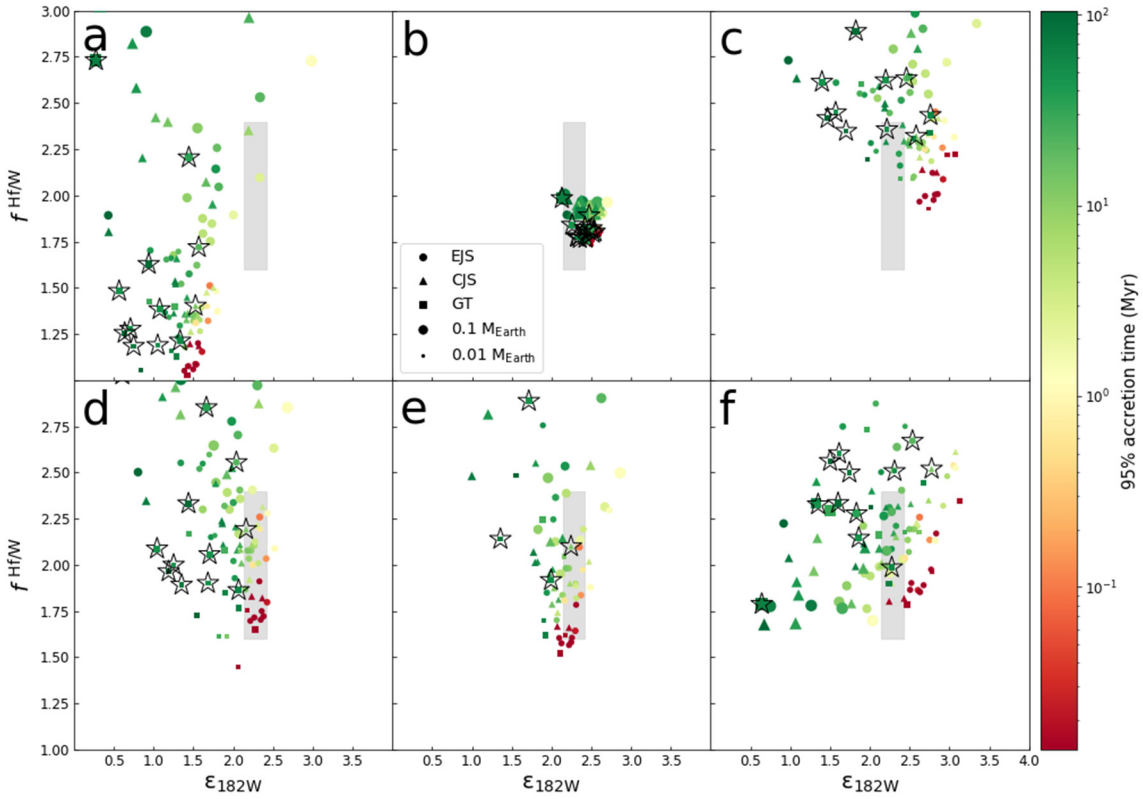


Alternate version of Figure 5 with relaxed parameter constraints. Symbol color indicates 95% accretion time, and symbol size is proportional to mass. Shaded grey region indicates the uncertainty range of measured Martian Shergotty-source values (Table S1). **a.** $fO_2$ = IW–1.2, 5.0 wt% S, $k_{mantle}$ = 1.0, $k_{core}$ = 1.0, $P_{frac}$ = 1.0, $\Delta T$ = 200 K. **b.** $fO_2$ = IW–1.7, 1.0 wt% S, $k_{mantle}$ = 0.1, $k_{core}$ = 0.1, $P_{frac}$ = 0.1, $\Delta T$ = –200 K. **c.** $fO_2$ = IW–1.7, 1.6 wt% S, $k_{mantle}$ = 0.4, $k_{core}$ = 0.85, $P_{frac}$ = 0.4, $\Delta T$ = –200 K. **d.** $fO_2$ = IW–1.5, 3.5 wt% S, $k_{mantle}$ = 0.4, $k_{core}$ = 0.85, $P_{frac}$ = 0.4, 5 Myr between CAI condensation and simulation start. **e.** Initial $fO_2$ of IW–4.0 inside 1.5 AU and IW –1.4 outside of 1.5 AU, 3.5 wt% S, $k_{mantle}$ = 0.4, $k_{core}$ = 0.85, $P_{frac}$ = 0.6, $\Delta T$ = 150 K. **f.** Reference case conditions calculated with Siebert et al. (2011) coefficients (i.e., Figure S4): $fO_2$ = IW –1.22, 3.5 wt% S, $k_{mantle}$ = 0.4, $k_{core}$ = 0.85, $P_{frac}$ = 0.6.

**Figure S4**

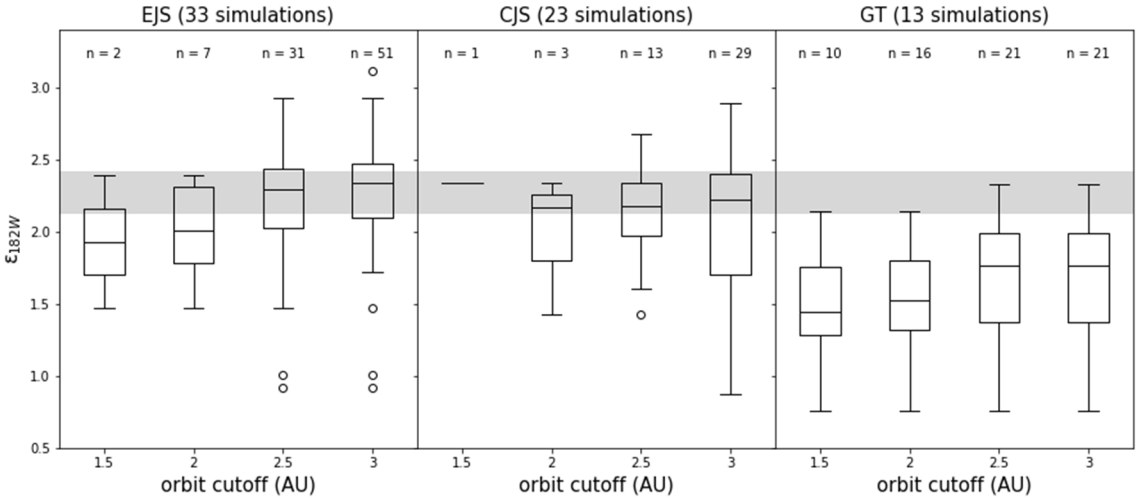


Orbital distribution of final analog $^{182}$W anomalies under "reference case" model conditions (Figure 5a; $fO_2$ = IW–1.47, 3.5 wt% S, $k_{mantle}$ = 0.4, $k_{core}$ = 0.85, $P_{frac}$ = 0.6). The shaded band indicates the measured Martian value with uncertainty (Table S4). As in Figure 2 of the main text, there does not appear to be a strong relationship between a body's final orbit and its final $\varepsilon_{182W}$. This implies that accretion history is independent of final analog orbit. For example, if analogs with more distant orbits took substantially longer to accrete, there would be a negative correlation between orbit cutoff and $\varepsilon_{182W}$.

**Table S1**

| element | abundance (wt%) | geochemistry |
|---|---|---|
| Fe | 43.78 | partitioned ($D_{Fe}$) |
| Si | 25.10 | perfectly lithophile |
| Mg | 22.38 | perfectly lithophile |
| Ni | 2.56 | partitioned ($D_{Fe}$) |
| Ca | 2.61 | perfectly lithophile |
| Al | 2.40 | perfectly lithophile |
| Na | 1.16 | perfectly lithophile |
| Hf | $3.06 \times 10^{-5}$ | perfectly lithophile |
| W | $2.75 \times 10^{-5}$ | partitioned ($D_W$) |
| S | variable (1.0–5.0) | perfectly siderophile |
| C | variable (0.0–0.2) | perfectly siderophile |

Bulk Mars composition used in this study. Compositions are from Palme & O'Neill (2014) and are based on a CI chondrite with oxygen and the highly volatile elements removed. Bulk S was varied in the range 1–5 wt% and compositions were renormalized to 100 wt% for each analog. Bulk C was fixed at 0 wt% except in one instance (Section 3.3). Note that Si is unlikely to be "perfectly lithophile" in planets larger or more reducing than Mars (e.g., Lin et al., 2002; Georg et al., 2007).

**Table S2**

| parameter | Jennings et al. (2021) | Siebert et al. (2011) | Wade et al. (2012) |
|---|---|---|---|
| *a* | 0.61(28) | 1.96(14) | 1.80(24) |
| *b* | –4091(670) | –937(741) | –6728 |
| *c* | 0 | –55(35) | –77 |
| *d* | 0 | –0.57(4) | 0 |
| *n* | 6+ | 4+ | 6+ |

Metal–silicate partitioning parameters for W (Equation 5) from various studies with reported uncertainties. Major disagreements include the interpreted valence state (*n*), whether the pressure term (*c*) is statistically meaningful, and whether to parameterize melt composition with an $\frac{nbo}{t}$ term (*d*). We use the Jennings et al. (2021) values in our analysis. Compare Figure 4 with Figure S2 for an example of how the choice of partitioning parameters can influence the analogs' calculated Hf–W signatures.

**Table S3**

| analog ID | mass ($M_{Earth}$) | ecc. | SMA (AU) | prov. (AU) | $t_{50}$ (Myr) | $t_{95}$ (Myr) | planetesimals accreted | embryos accreted | $f^{Hf/W}$ | $\varepsilon_{182W}$ |
|---|---|---|---|---|---|---|---|---|---|---|
| EJS3:65 | 0.0593 | 0.229 | 2.33 | 2.75 | 0 | 8.66 | 9 | 0 | 2.02 | 2.34 |
| EJS7:55 | 0.1060 | 0.148 | 2.24 | 1.95 | 0.19 | 42.86 | 25 | 1 | 2.82 | 2.41 |
| EJS8:63 | 0.1150 | 0.149 | 2.85 | 2.39 | 0.25 | 2.54 | 17 | 1 | 2.74 | 3.12 |
| EJS9:52 | 0.0489 | 0.348 | 1.73 | 1.83 | 0 | 48.50 | 11 | 0 | 2.06 | 1.81 |
| EJS9:64 | 0.0521 | 0.159 | 2.94 | 2.68 | 0 | 0 | 2 | 0 | 1.74 | 2.34 |
| EJS10:67 | 0.0670 | 0.209 | 2.68 | 2.89 | 0 | 0.10 | 13 | 0 | 2.24 | 2.57 |
| EJS11:61 | 0.1080 | 0.135 | 1.91 | 2.17 | 5.15 | 5.15 | 10 | 1 | 2.49 | 2.33 |
| EJS16:51 | 0.0471 | 0.555 | 2.27 | 1.83 | 0 | 6.21 | 10 | 0 | 2.02 | 2.44 |
| EJS16:63 | 0.0549 | 0.098 | 2.53 | 2.54 | 0 | 42.68 | 6 | 0 | 1.92 | 2.10 |
| EJS18:49 | 0.1770 | 0.020 | 2.03 | 1.77 | 1.36 | 69.40 | 13 | 3 | 3.29 | 1.72 |
| EJS18:53 | 0.0608 | 0.005 | 1.00 | 1.66 | 0 | 40.82 | 22 | 0 | 2.43 | 1.47 |
| EJS21:53 | 0.1470 | 0.099 | 2.39 | 2.26 | 0.19 | 10.78 | 9 | 2 | 2.85 | 2.23 |
| EJS22:52 | 0.0499 | 0.174 | 2.85 | 1.88 | 0 | 0.63 | 12 | 0 | 2.10 | 2.54 |
| EJS23:62 | 0.0497 | 0.261 | 2.22 | 2.51 | 0 | 0.00 | 2 | 0 | 1.72 | 2.43 |
| EJS23:65 | 0.0613 | 0.101 | 2.57 | 2.69 | 0 | 3.54 | 10 | 0 | 2.10 | 2.46 |
| EJS24:65 | 0.0684 | 0.290 | 2.32 | 2.57 | 0 | 14.10 | 17 | 0 | 2.36 | 2.30 |
| EJS25:56 | 0.0555 | 0.066 | 2.24 | 2.05 | 0 | 1.30 | 14 | 0 | 2.20 | 2.68 |
| EJS26:54 | 0.1080 | 0.106 | 1.55 | 1.75 | 2.81 | 35.04 | 29 | 1 | 2.90 | 2.01 |
| EJS26:60 | 0.0485 | 0.061 | 2.52 | 2.35 | 0 | 0 | 3 | 0 | 1.75 | 2.46 |
| EJS26:61 | 0.0486 | 0.096 | 2.11 | 2.38 | 0 | 0 | 2 | 0 | 1.71 | 2.27 |
| EJS26:64 | 0.0591 | 0.129 | 2.55 | 2.61 | 0 | 10.07 | 9 | 0 | 2.06 | 2.39 |
| EJS26:65 | 0.0593 | 0.144 | 2.14 | 2.75 | 0 | 0.14 | 8 | 0 | 2.02 | 2.60 |
| EJS27:67 | 0.0690 | 0.051 | 2.07 | 2.79 | 0 | 34.30 | 16 | 0 | 2.31 | 2.19 |
| EJS28:63 | 0.1010 | 0.072 | 2.24 | 2.17 | 3.02 | 4.90 | 7 | 1 | 2.39 | 2.31 |
| EJS28:64 | 0.1790 | 0.256 | 2.39 | 2.39 | 0.17 | 26.46 | 22 | 2 | 3.57 | 2.53 |
| EJS29:51 | 0.0994 | 0.036 | 2.02 | 1.66 | 0.69 | 21.84 | 22 | 1 | 2.73 | 2.50 |
| EJS29:66 | 0.1710 | 0.033 | 2.64 | 2.86 | 0.12 | 1.29 | 10 | 2 | 3.14 | 3.55 |
| EJS30:61 | 0.0546 | 0.046 | 2.29 | 2.37 | 0 | 35.28 | 10 | 0 | 1.99 | 2.11 |
| EJS31:37 | 0.0387 | 0.133 | 2.05 | 1.28 | 0 | 31.55 | 11 | 0 | 2.02 | 1.88 |
| EJS31:64 | 0.0591 | 0.169 | 2.56 | 2.55 | 0 | 12.98 | 9 | 0 | 2.06 | 2.34 |
| EJS33:42 | 0.0839 | 0.141 | 2.54 | 1.59 | 8.00 | 8.00 | 13 | 1 | 2.31 | 1.92 |
| EJS34:31 | 0.0949 | 0.174 | 2.61 | 1.08 | 0.03 | 16.72 | 40 | 1 | 2.99 | 2.43 |
| EJS35:50 | 0.1350 | 0.230 | 2.25 | 1.66 | 0.05 | 19.88 | 24 | 2 | 3.12 | 2.93 |
| EJS35:58 | 0.0585 | 0.442 | 2.43 | 2.09 | 0 | 17.76 | 15 | 0 | 2.24 | 2.05 |
| EJS36:35 | 0.0487 | 0.411 | 2.57 | 1.25 | 0 | 40.27 | 22 | 0 | 2.37 | 1.81 |
| EJS37:62 | 0.1060 | 0.355 | 2.80 | 2.44 | 0.03 | 1.98 | 10 | 1 | 2.50 | 2.72 |
| EJS38:67 | 0.1020 | 0.018 | 2.67 | 2.35 | 0 | 4.28 | 9 | 1 | 2.44 | 2.47 |
| EJS39:53 | 0.0983 | 0.137 | 2.25 | 1.51 | 11.29 | 189.28 | 19 | 1 | 2.54 | 0.92 |
| EJS39:58 | 0.0494 | 0.118 | 2.22 | 2.19 | 0 | 0 | 18 | 0 | 1.88 | 2.46 |
| EJS40:61 | 0.0516 | 0.196 | 2.28 | 2.41 | 0 | 12.06 | 5 | 0 | 1.85 | 2.25 |
| EJS40:68 | 0.0583 | 0.133 | 2.70 | 3.04 | 0 | 0.02 | 3 | 0 | 1.83 | 2.56 |

| analog ID | mass ($M_{Earth}$) | ecc. | SMA (AU) | prov. (AU) | $t_{50}$ (Myr) | $t_{95}$ (Myr) | planetesimals accreted | embryos accreted | $f^{Hf/W}$ | $\varepsilon_{182W}$ |
|---|---|---|---|---|---|---|---|---|---|---|
| EJS42:68 | 0.0623 | 0.334 | 1.15 | 3.00 | 0 | 0.59 | 7 | 0 | 2.01 | 2.40 |
| EJS43:67 | 0.0629 | 0.050 | 2.89 | 2.94 | 0 | 1.11 | 9 | 0 | 2.08 | 2.75 |
| EJS44:27 | 0.0469 | 0.160 | 2.64 | 0.93 | 0 | 17.89 | 24 | 0 | 2.41 | 1.92 |
| EJS44:57 | 0.0645 | 0.123 | 1.54 | 2.01 | 0 | 20.93 | 22 | 0 | 2.46 | 2.29 |
| EJS44:69 | 0.1150 | 0.203 | 2.44 | 2.84 | 0 | 9.62 | 10 | 1 | 2.57 | 2.11 |
| EJS46:65 | 0.0533 | 0.274 | 2.72 | 2.75 | 0 | 0 | 2 | 0 | 1.75 | 2.48 |
| EJS48:45 | 0.0537 | 0.274 | 1.97 | 1.46 | 0 | 24.52 | 21 | 0 | 2.37 | 1.74 |
| EJS48:68 | 0.1100 | 0.151 | 2.99 | 2.74 | 0 | 4.75 | 2 | 1 | 2.30 | 2.47 |
| EJS50:45 | 0.1990 | 0.696 | 2.47 | 1.39 | 19.62 | 63.81 | 32 | 1 | 4.09 | 1.01 |
| EJS50:55 | 0.0485 | 0.863 | 2.36 | 2.01 | 0 | 4.05 | 8 | 0 | 1.95 | 2.47 |
| CJS4:24 | 0.1310 | 0.326 | 2.43 | 1.51 | 5.07 | 16.76 | 35 | 2 | 3.08 | 1.60 |
| CJS5:72 | 0.0642 | 0.448 | 2.89 | 3.48 | 0 | 0 | 3 | 0 | 1.88 | 2.33 |
| CJS7:58 | 0.0534 | 0.203 | 2.84 | 2.22 | 0 | 6.84 | 10 | 0 | 2.05 | 2.40 |
| CJS7:65 | 0.0603 | 0.555 | 1.54 | 2.68 | 0 | 29.90 | 9 | 0 | 2.06 | 2.17 |
| CJS8:57 | 0.1040 | 0.212 | 2.23 | 2.11 | 0.68 | 34.18 | 15 | 1 | 2.60 | 2.40 |
| CJS8:66 | 0.0616 | 0.101 | 2.53 | 2.82 | 0 | 9.89 | 9 | 0 | 2.07 | 2.23 |
| CJS8:70 | 0.0652 | 0.110 | 2.16 | 3.20 | 0 | 14.21 | 7 | 0 | 2.03 | 2.22 |
| CJS9:51 | 0.1620 | 0.251 | 2.82 | 1.92 | 0.01 | 22.32 | 35 | 2 | 3.58 | 2.74 |
| CJS10:71 | 0.0647 | 0.023 | 2.61 | 3.33 | 0 | 3.67 | 5 | 0 | 1.96 | 2.32 |
| CJS11:53 | 0.0508 | 0.122 | 1.47 | 1.97 | 0 | 11.94 | 12 | 0 | 2.11 | 2.34 |
| CJS11:58 | 0.1010 | 0.305 | 2.66 | 1.98 | 24.82 | 69.62 | 11 | 1 | 2.42 | 1.00 |
| CJS11:71 | 0.0627 | 0.135 | 2.87 | 3.34 | 0 | 0.00 | 3 | 0 | 1.87 | 2.49 |
| CJS12:45 | 0.1020 | 0.192 | 2.65 | 1.40 | 12.50 | 40.68 | 34 | 1 | 2.91 | 1.33 |
| CJS12:66 | 0.0707 | 0.495 | 2.10 | 2.71 | 0 | 40.10 | 18 | 0 | 2.40 | 1.95 |
| CJS13:71 | 0.1260 | 0.078 | 2.86 | 3.10 | 3.17 | 16.74 | 9 | 1 | 2.66 | 2.31 |
| CJS16:67 | 0.0660 | 0.664 | 2.48 | 2.87 | 0.00 | 2.73 | 13 | 0 | 2.20 | 2.52 |
| CJS18:50 | 0.1580 | 0.075 | 2.03 | 1.81 | 0.10 | 41.77 | 45 | 2 | 3.73 | 2.68 |
| CJS18:63 | 0.0609 | 0.244 | 2.34 | 2.55 | 0 | 36.04 | 12 | 0 | 2.16 | 2.18 |
| CJS19:68 | 0.1690 | 0.034 | 1.94 | 2.22 | 8.84 | 42.00 | 20 | 2 | 3.30 | 1.43 |
| CJS21:60 | 0.0555 | 0.224 | 2.29 | 2.29 | 0 | 49.75 | 10 | 0 | 2.06 | 1.98 |
| CJS23:72 | 0.0733 | 0.331 | 2.27 | 3.30 | 0 | 55.45 | 12 | 0 | 2.25 | 1.98 |
| CJS28:53 | 0.0538 | 0.147 | 2.88 | 1.94 | 0 | 3.46 | 15 | 0 | 2.21 | 2.62 |
| CJS30:76 | 0.1970 | 0.108 | 2.67 | 3.06 | 12.01 | 35.20 | 24 | 2 | 3.83 | 1.62 |
| CJS31:59 | 0.0545 | 0.316 | 2.31 | 2.25 | 0 | 24.10 | 10 | 0 | 2.06 | 2.23 |
| CJS32:65 | 0.1280 | 0.217 | 2.98 | 2.65 | 0.31 | 7.76 | 23 | 1 | 3.02 | 2.89 |
| CJS37:40 | 0.1400 | 0.382 | 2.77 | 1.58 | 8.47 | 12.00 | 21 | 2 | 2.98 | 1.70 |
| CJS40:69 | 0.1940 | 0.214 | 2.88 | 2.42 | 19.60 | 175.43 | 16 | 2 | 3.45 | 0.87 |
| CJS48:76 | 0.0791 | 0.459 | 2.79 | 3.82 | 0 | 62.47 | 11 | 0 | 2.27 | 1.97 |
| CJS49:73 | 0.1470 | 0.137 | 2.83 | 2.88 | 18.96 | 40.88 | 26 | 1 | 3.24 | 1.32 |
| GT1:38 | 0.0543 | 0.115 | 2.14 | 2.81 | 0 | 62.64 | 6 | 0 | 1.79 | 2.12 |
| GT2:26 | 0.0567 | 0.030 | 1.46 | 1.89 | 0 | 55.91 | 6 | 0 | 1.87 | 2.15 |
| GT2:38 | 0.0518 | 0.160 | 2.17 | 2.86 | 0 | 0 | 5 | 0 | 1.68 | 2.33 |
| GT5:40 | 0.0617 | 0.117 | 1.43 | 2.76 | 0 | 44.47 | 7 | 0 | 2.05 | 1.76 |

| analog ID | mass ($M_{Earth}$) | ecc. | SMA (AU) | prov. (AU) | $t_{50}$ (Myr) | $t_{95}$ (Myr) | planetesimals accreted | embryos accreted | $f^{Hf/W}$ | $\varepsilon_{182W}$ |
|---|---|---|---|---|---|---|---|---|---|---|
| GT6:10 | 0.1634 | 0.027 | 1.01 | 1.45 | 0.35 | 28.79 | 63 | 0 | 4.14 | 1.81 |
| GT7:30 | 0.0697 | 0.043 | 1.41 | 2.17 | 0 | 94.99 | 13 | 0 | 2.30 | 1.52 |
| GT8:30 | 0.0620 | 0.287 | 1.68 | 2.20 | 0 | 24.32 | 18 | 0 | 2.07 | 1.99 |
| GT9:43 | 0.0332 | 0.073 | 1.89 | 1.82 | 0 | 57.59 | 15 | 0 | 1.76 | 1.97 |
| GT9:74 | 0.0359 | 0.045 | 1.47 | 2.53 | 0 | 110.90 | 5 | 0 | 1.86 | 1.18 |
| GT10:18 | 0.1586 | 0.048 | 1.26 | 1.45 | 0.82 | 63.91 | 61 | 1 | 4.06 | 1.37 |
| GT10:41 | 0.0283 | 0.195 | 2.01 | 1.67 | 0 | 11.35 | 3 | 0 | 1.56 | 1.91 |
| GT10:43 | 0.0310 | 0.466 | 2.18 | 1.80 | 0 | 0.01 | 4 | 0 | 1.68 | 2.25 |
| GT11:33 | 0.0257 | 0.235 | 2.06 | 1.45 | 0 | 0.00 | 1 | 0 | 1.41 | 2.01 |
| GT11:37 | 0.0624 | 0.042 | 1.52 | 1.72 | 0.06 | 44.89 | 9 | 1 | 2.05 | 1.14 |
| GT12:24 | 0.0413 | 0.111 | 1.79 | 1.47 | 0 | 26.47 | 10 | 0 | 2.04 | 1.53 |
| GT12:33 | 0.0283 | 0.251 | 1.88 | 1.57 | 0 | 24.02 | 3 | 0 | 1.56 | 1.79 |
| GT14:15 | 0.1741 | 0.069 | 1.49 | 1.53 | 43.99 | 63.80 | 24 | 2 | 3.31 | 0.76 |
| GT14:69 | 0.0307 | 0.030 | 1.74 | 2.49 | 0 | 117.00 | 2 | 0 | 1.65 | 1.51 |
| GT15:45 | 0.0338 | 0.033 | 1.41 | 1.85 | 0 | 72.49 | 7 | 0 | 1.79 | 1.34 |
| GT16:50 | 0.0339 | 0.082 | 1.48 | 2.01 | 0 | 48.89 | 8 | 0 | 1.80 | 1.73 |
| GT16:52 | 0.0364 | 0.073 | 1.45 | 1.98 | 0 | 45.03 | 16 | 0 | 1.89 | 1.26 |

Analog properties. Mass, eccentricity (ecc.), semi-major axis (SMA), and Hf–W values are given at the end of the *N*-body simulation. Provenance (prov.) is the mass-weighted average of the initial semi-major axes of the analog's building blocks. Times are given in simulation time (starting 2 Myr after CAI formation), with $t_{50}$ and $t_{95}$ being the times at which the analog reached 50% and 95% of its final mass, respectively (a value of 0 indicates that the threshold was reached before the start of the simulation). Counts of accreted bodies only include planetesimals and embryos that impacted the analog itself, and do not include the seed embryo or any bodies that had previously impacted its impactors. Hf–W evolution was calculated at "reference case" conditions (Figure 5a; $fO_2$ = IW–1.47, 3.5 wt% S, $k_{mantle}$ = 0.4, $k_{core}$ = 0.85, $P_{frac}$ = 0.6).

**Table S4**

| Parameter | Value | Source |
|---|---|---|
| $\left({}^{180}\mathrm{Hf}/{}_{184}\mathrm{W}\right)_{CHUR}$ | 1.35 ± 0.11 | Kleine & Walker (2017) |
| $t_{1/2}$ of $^{182}$Hf | 8.9 ± 0.1 Myr | Kleine & Walker (2017) |
| $t_{CAI}$ | 4.567 Ga | MacPherson (2014) |
| $\left({}^{182}\mathrm{Hf}/{}_{180}\mathrm{Hf}\right)_{inital}$ | (1.018 ± 0.043) × $10^{-4}$ | Kruijer et al. (2014) |
| $\left({}^{182}\mathrm{W}/{}_{184}\mathrm{W}\right)_{inital}$ | 0.865 ± 0.001 | Kruijer et al. (2014) |
| $\left({}^{184}\mathrm{W}/{}_{\mathrm{W}}\right)_{modern}$ | 0.3064 ± 0.0002 | IUPAC (2003) |
| $\left({}^{180}\mathrm{Hf}/{}_{\mathrm{Hf}}\right)_{modern}$ | 0.3508 ± 0.0016 | IUPAC (2003) |
| Martian mantle $f^{\mathrm{Hf/W}}$ | 2.0 ± 0.4 | Kleine & Walker (2017) |
| Martian mantle $\varepsilon_{182\mathrm{W}}$ (relative to terrestrial) | 0.37 ± 0.04 | Kruijer et al. (2017) |
| CHUR $\varepsilon_{182\mathrm{W}}$ (relative to terrestrial) | –1.9 ± 0.1 | Kleine & Walker (2017) |

Values used for the Hf–W isotopic calculations. Formulations of $\varepsilon_{182\mathrm{W}}$ and $f^{\mathrm{Hf/W}}$ are given in Equations 1 and 2, respectively. In this study, we compare our analogs to $\varepsilon_{182\mathrm{W}}$ of the Martian mantle relative to the chondritic reservoir CHUR (2.27 ± 0.14), which is equal to the difference between the Martian mantle $\varepsilon_{182\mathrm{W}}$ and CHUR $\varepsilon_{182\mathrm{W}}$ values listed here.

**Supplementary References**


Georg R. B., Halliday A. N., Schauble E. A. and Reynolds B. C. (2007) Silicon in the Earth's core. *Nature* **447**, 1102–1106.

International Union of Pure and Applied Chemistry (2003) Atomic weights of the elements: Review 2000. *Pure Appl. Chem.* **75**, 683–800.

Jacobsen S. B. (2005) The Hf-W isotopic system and the origin of the Earth and Moon. *Annu. Rev. Earth Planet. Sci* **33**, 531–70.

Jennings E. S., Jacobson S. A., Rubie D. C., Nakajima Y., Vogel A. K., Rose-Weston L. A. and Frost D. J. (2021) Metal–silicate partitioning of W and Mo and the role of carbon in controlling their abundances in the bulk silicate earth. *Geochim. Cosmochim. Acta* **293**, 40–69.

Kleine T. and Walker R. J. (2017) Tungsten Isotopes in Planets. *Annu. Rev. Earth Planet. Sci.* **45**, 389–417.

Kruijer T. S., Kleine T., Fischer-Gödde M., Burkhardt C. and Wieler R. (2014) Nucleosynthetic W isotope anomalies and the Hf-W chronometry of Ca-Al-rich inclusions. *Earth Planet. Sci. Lett.* **403**, 317–327.

Kruijer T. S., Kleine T., Borg L. E., Brennecka G. A., Irving A. J., Bischoff A. and Agee C. B. (2017) The early differentiation of Mars inferred from Hf–W chronometry. *Earth Planet. Sci. Lett.* **474**, 345–354.

Lin J. F., Heinz D. L., Campbell A. J., Devine J. M. and Shen G. (2002) Iron-silicon alloy in earth's core? *Science* **295**, 313–315.

MacPherson G. J. (2014) Calcium-aluminum-rich inclusions in chondritic meteorites. *Meteorites Cosmochem. Process.*, 139–179.

Morishima R., Golabek G. J. and Samuel H. (2013) N-body simulations of oligarchic growth of Mars: Implications for Hf-W chronology. *Earth Planet. Sci. Lett.* **366**, 6–16.

Nimmo F. and Kleine T. (2007) How rapidly did Mars accrete? Uncertainties in the Hf–W timing of core formation. *Icarus* **191**, 497–504.

Palme H. and O'Neill H. S. C. (2014) Cosmochemical Estimates of Mantle Composition. In *Treatise on Geochemistry* **3.1**, 1–39.

Siebert J., Corgne A. and Ryerson F. J. (2011) Systematics of metal-silicate partitioning for many siderophile elements applied to Earth's core formation. *Geochim. Cosmochim. Acta* **75**, 1451–1489.

Wade J., Wood B. J. and Tuff J. (2012) Metal–silicate partitioning of Mo and W at high pressures and temperatures: Evidence for late accretion of sulphur to the Earth. *Geochim. Cosmochim. Acta* **85**, 58–74.